Electronic Supplementary Material (ESI) for Materials Horizons.

Supporting Information

Rational design of zinc powder anode with high utilization and long cycle life for advanced aqueous Zn–S batteries

Jianbo Li, Zexiao Cheng, Zhen Li*, Yunhui Huang*

State Key Laboratory of Material Processing and Die and Mold Technology, School of Materials Science and Engineering, Huazhong University of Science and Technology, Wuhan 430074, China

E-mail: li_zhen@hust.edu.cn; huangyh@hust.edu.cn

Experimental Section

Material: Zn powder (AR), $ZnSO_4$ $7H_2O$ (≥99.9%), ZnI_2 and $InCl_3$ (≥98%) were purchased from Shanghai Aladdin Biochemical Technology Co., Ltd; CMK-3, CNT were purchased from Nanjing Jicang Nano Co. Ltd; sulfur was purchased from Sigma-Aldrich; polytetrafluoroethylene (PTFE) and Ketjen Black (KB) were purchased from Guangdong Canrd New Energy Technology Co., Ltd.

Preparation of pZn/In: The indium-modified powder Zn (pZn/In) was prepared by the chemical substitution reaction. Typically, 221 mg of $InCl_3$ was added into 10.0 mL of ultra-pure water under ultrasonication. Then, 15 mL of ultra-pure water solution containing 0.5 g Zn powder was poured into the above solution and stirred for 1 min. Afterward, the obtained pZn/In was filtered and washed with ultra-pure water and ethanol. Finally, the product was dried at 60 °C for 6 h. As comparisons, pZn/In with different concentrations of $InCl_3$ (0.05 M or 0.15 M) was synthesized by the same method as above. The obtained samples are named as pZn/In-1 and pZn/In-2, respectively.

Preparation of pZn/In anode: The pZn/In (85 wt.%), conductive (10 wt.%, KB: CNT=7:3) and PTFE (5 wt.%) were mixed in isopropanol and then ground for 30 min. After that, the mixture was mechanically processed into a thin film, followed by drying in a vacuum at 60 °C for 8 h to obtain the pZn/In anode.

Preparation of CMK-3/S or KB/S cathode: The CMK-3 or KB and S powder were mixed at a mass ratio of 6:4 and then ground for 30 min. After that, the mixture was put into a glass tube for heat treatment at 155 °C for 12 h under a vacuum. The as-prepared cathode was mixed with 80 wt.% CMK-3/S or KB/S, 10 wt.% KB and 10 wt.% PTFE in isopropanol for 15 min, mechanically processed into a thin film, and then pressed onto stainless steel mesh current collector. Finally, the above electrode was dried in vacuum at 70 °C for 12 h to obtain the CMK-3/S or KB/S cathode. The loading of S is 2.0∼2.5 mg cm^{-2}.

Characterization Methods

The morphology investigation used a Sirion 200 instrument field-emission scanning electron microscopy (SEM, with an accelerating voltage of 20 kV) and field emission transmission electron microscope (F-TEM, Tecnai G2 F30, FEI, Hillsboro, OR, USA) equipped with EDS. The X-ray diffraction patterns (XRD) of the samples (scan range: 5°–80°, scan step: 10° min^{-1}) were collected by X-ray powder diffractometry (PANalytical X'Pert PRODY2198, Holland), operating at 40 kV and 40 mA with Cu Kα radiation (λ = 0.15406 nm). Elemental analysis was performed on a CHNS elemental analyzer (Vario Micro cube, Elementar). The thermogravimetric analysis (TGA) was measured from 40 to 800 °C with a heating rate of 10 °C min^{-1} under an N_2 flow to calculate the content of S (STA449 F3 Jupiter thermogravimetric analyzer (NETZSCH)). The *in-situ* observations of Zn deposition and exfoliation were carried out on an optical microscope (6XB-PC, Optical Instrument Factory), where the pZn anode was fixed onto a transparent glass plate to construct a homemade optical cell.

Electrochemical measurements

The asymmetric Zn||Cu-type batteries were assembled using Cu as the counter/reference electrode and pZn/In as the working electrode, while the symmetric Zn||Zn type symmetric cells were assembled using pZn/In or bare pZn as both the working electrode and the counter/reference electrode. The full batteries with CMK-3/S cathode were assembled using pZn/In electrode as the anode, glass fiber membrane as the separator, 2 M $ZnSO_4$ aqueous solution with 20 mM ZnI_2 as electrolyte. The cell was sealed in air and left for 12 h before electrochemical tests. Galvanostatic discharge/charge measurements of asymmetric, symmetric, full cells were performed on a LAND battery-testing instrument. Before measuring the cycle performance, all the full cells are activated for 3 cycles at 0.1 C.

The n/p ratio for calculating the energy density was used according to the previous study.

Gravimetric Energy Density (Wh kg^{-1})

$$E_g = \frac{U \cdot m_A \cdot C_S}{n \cdot m_{cathode} + m_{anode}}$$

Where U, m_A, and C_S represent the average cell voltage (V), the areal mass loading of cathode active material (g cm^{-2}), and the specific capacity of the cell (mAh g^{-1}), respectively. $m_{cathode}$ and m_{anode} describes the areal mass (g cm^{-2}) of the cathode and anode, respectively. n denotes the value of n in the N/P ratio.

Volumetric Energy Density (Wh L^{-1})

$$E_v = \frac{U \cdot m_A \cdot C_S}{n \cdot V_{cathode} + V_{anode}}$$

where U, m_A, and C_S represent the average cell voltage (V), the areal mass loading of cathode active material (g cm^{-2}), and the specific capacity of the cell (mAh cm^{-3}), respectively. $V_{cathode}$ and V_{anode} describe the volume of the cathode and anode, respectively. n denotes the value of n in the n/p ratio.

Density Functional Theory Calculations:

The first-principles calculations were conducted using generalized gradient approximation and Perdew–Burke–Ernzerhof (GGA–PBE) in the Vienna Ab initio Simulation Package (VASP). The conjugated gradient method was utilized to optimize the geometry with the convergence threshold of 10^{-5} eV in energy and 0.01 eV Å^{-1} in force, respectively. The substrate surface (In (002) and Zn (002)) with a four-layer supercell and releasable top two-layer atoms was used during simulation. A vacuum region of 15 Å is applied to avoid interactions between the neighboring configurations. The binding energy (E_b) was calculated by the following equation:

$$E_b = E_{total} - E_{sub} - E_{Zn}$$

E_{total}, E_{sub}, and E_{Zn} represent the total energy of Zn and In substrate combined with Zn^{2+}, the energy of the substrate and the energy of the Zn atom, respectively.

Fig. S

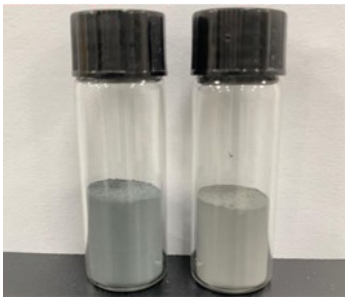

Fig. S1. The digital photograph of pZn (left) and pZn/In (right).

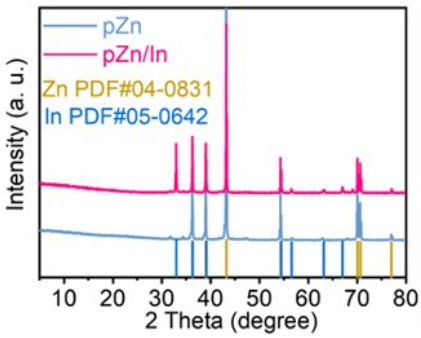

Fig. S2. The related XRD patterns for bare pZn and pZn/In.

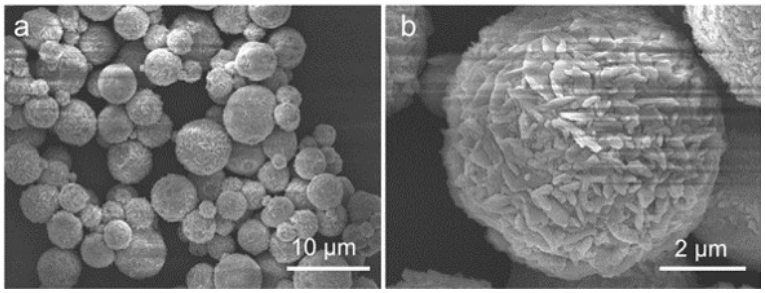

Fig. S3. SEM images of the surface of bare pZn.

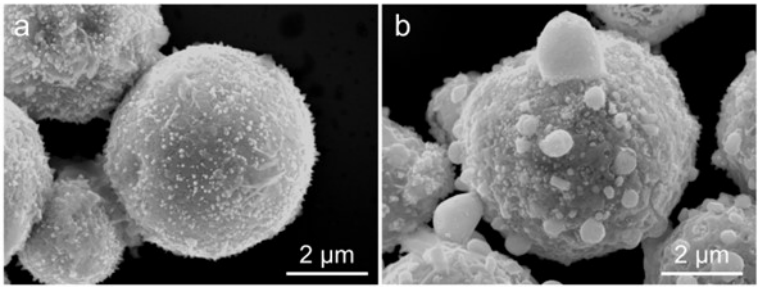

Fig. S4. SEM images of the surface of (a) pZn/In-1 and (a) pZn/In-2.

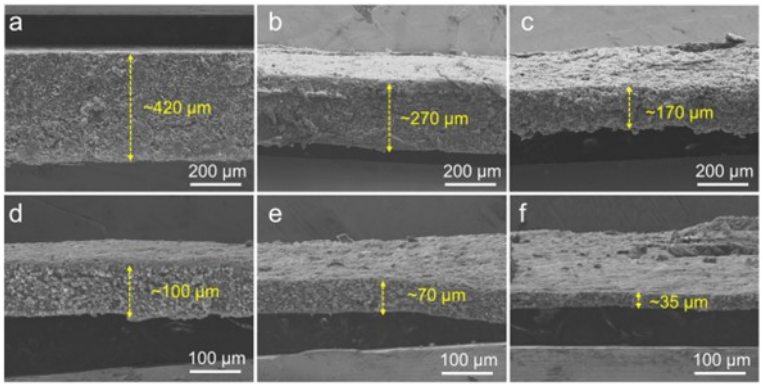

Fig. S5. The pZn/In anode with various thicknesses was obtained by using the rolling machine.

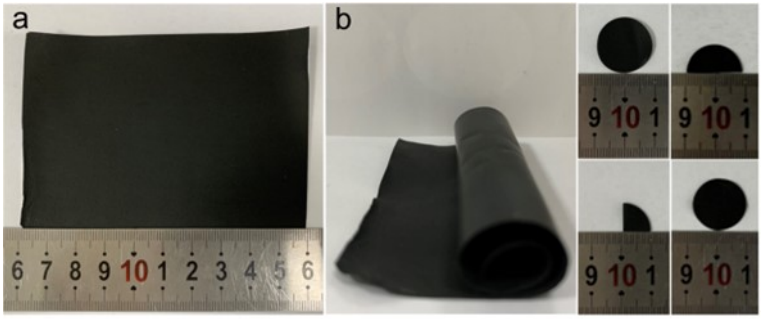

Fig. S6. (a) The digital photograph of pZn/In electrodes with the size of 10 × 8 cm^{-2}, and (b) the pZn/In electrodes at volume, folded, double folded and recover states.

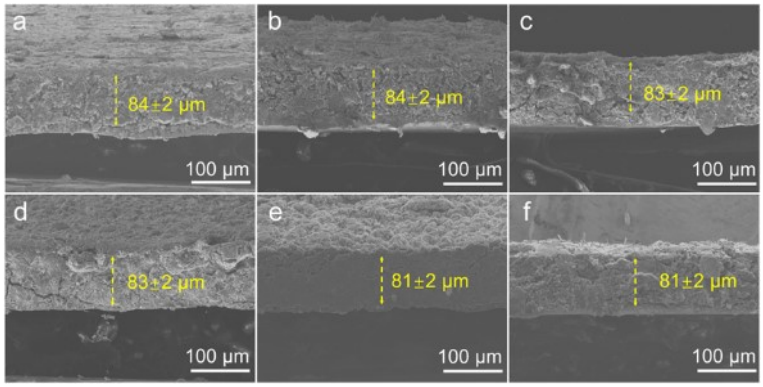

Fig. S7. The thickness of pZn/In anode during the Zn stripping process. (a) initial state with ~8mAh cm^{-2} of Zn), (b) 6.3% stripping (0.5 mAh cm^{-2}), (b) 12.5% stripping (1.0 mAh cm^{-2}), (c) 25% stripping (2.0

mAh cm^{-2}), (d) 37.5% stripping (3.0 mAh cm^{-2}), (e) 50% stripping (4.0 mAh cm^{-2}), (f) 62.5% stripping (5.0 mAh cm^{-2}), respectively.

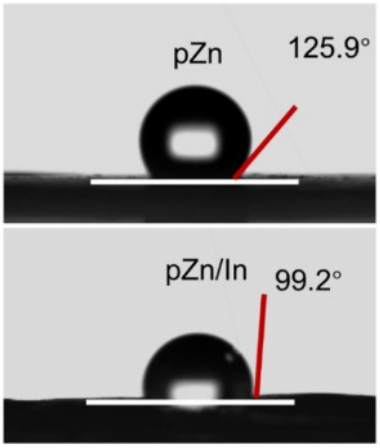

Fig. S8. Contact angles of 2 M $ZnSO_4$ electrolyte on pZn and pZn/In electrodes, respectively.

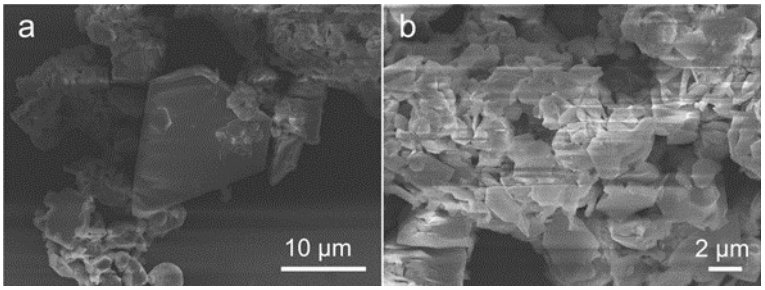

Fig. S9. SEM of bare pZn after immersion in 2 M $ZnSO_4$ for one week.

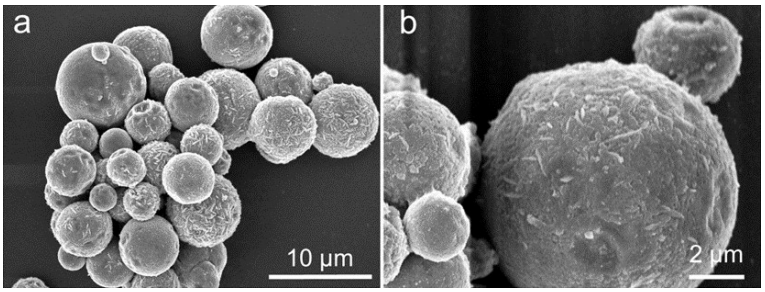

Fig. S10. SEM of pZn/In after immersion in 2 M $ZnSO_4$ for one week.

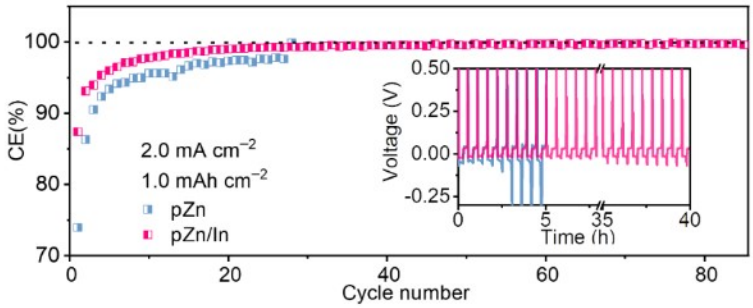

Fig. S11. CE and the related charge–discharge voltage profiles of Zn plating/stripping on pZn||Cu and pZn/In||Cu half cells at 2.0 mA cm^{-2} with 1.0 mAh cm^{-2}.

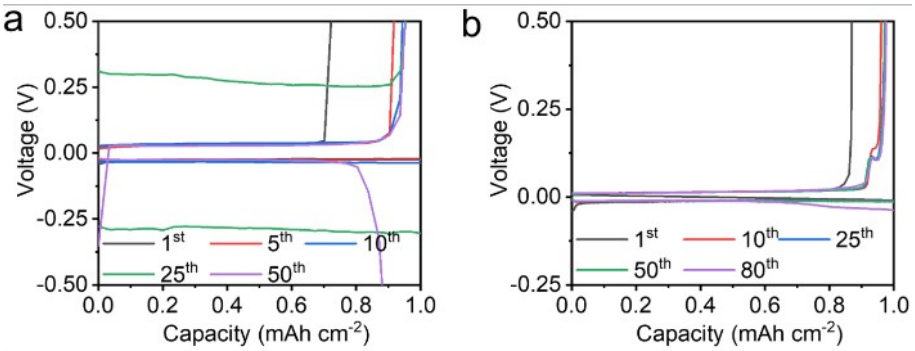

Fig. S12. The charge–discharge voltage profiles of Zn plating/stripping on (a) Cu||pZn and (b) Cu||pZn/In half cells at 2.0 mA cm^{-2} with 1.0 mAh cm^{-2}.

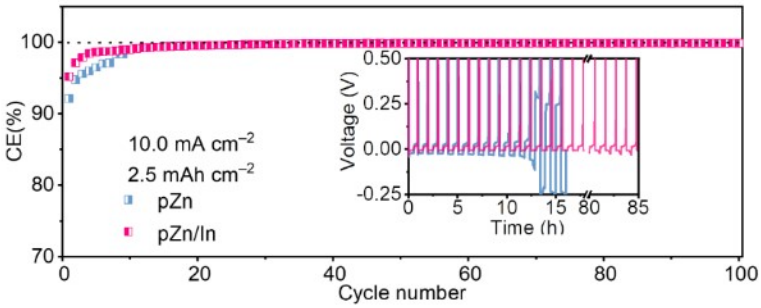

Fig. S13. CE and the related charge–discharge voltage profiles of Zn plating/stripping on pZn||Cu and pZn/In||Cu half cells at 10.0 mA cm^{-2} with 2.5 mAh cm^{-2}.

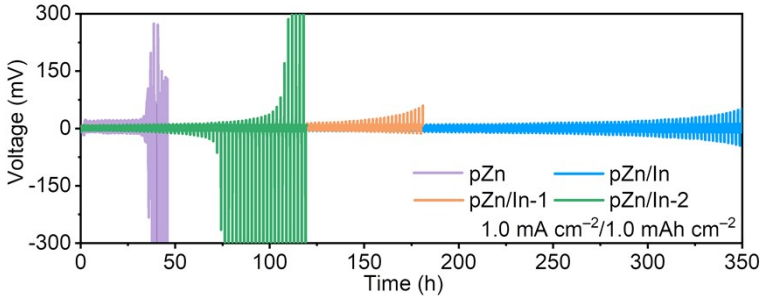

Fig. S14. Long-term galvanostatic cycling of Zn||Zn symmetric cells with different Zn electrodes at a current density of 1.0 mA cm^{-2} and a capacity of 1.0 mAh cm^{-2}.

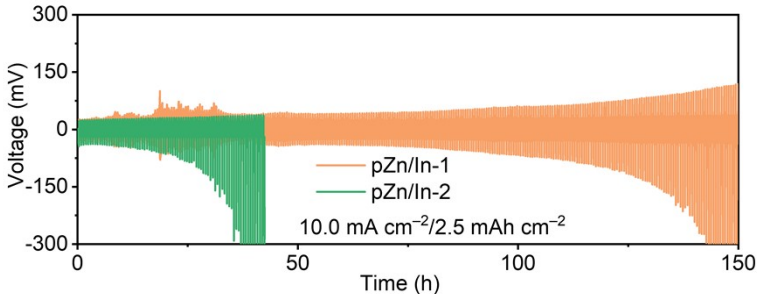

Fig. S15. The symmetrical cells with pZn/In-1 and pZn/In-2 electrodes at 10.0 mA cm^{-2} and a capacity of 2.5 mAh cm^{-2}.

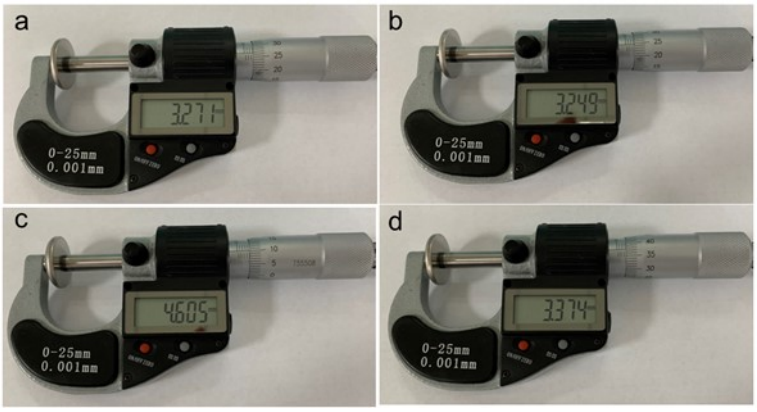

Fig. S16. The thickness variation of Zn||Zn symmetric cells after cycling. The freshly assembled Zn||Zn symmetric cells with (a) pZn anode, (b) pZn/In anode; the corresponding thickness of Zn||Zn symmetric cells with (c) pZn anode after 30 cycles, (d) pZn/In anode after 200 cycles, respectively, under the current density of 2 mA cm^{-2} with a capacity of 1 mAh cm^{-2}.

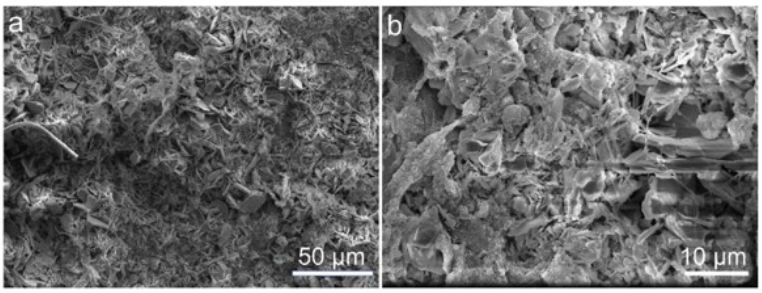

Fig. S17. SEM images of pZn anode after cycles.

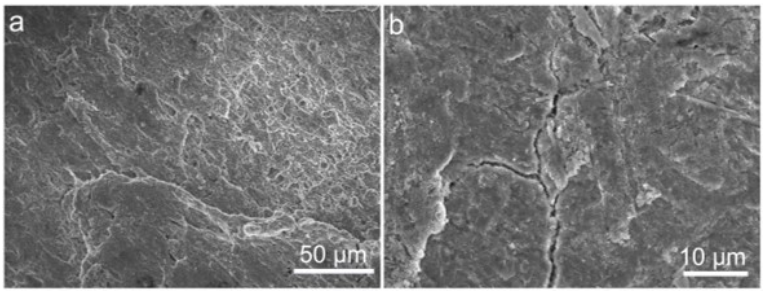

Fig. S18. SEM images of pZn/In anode after cycles.

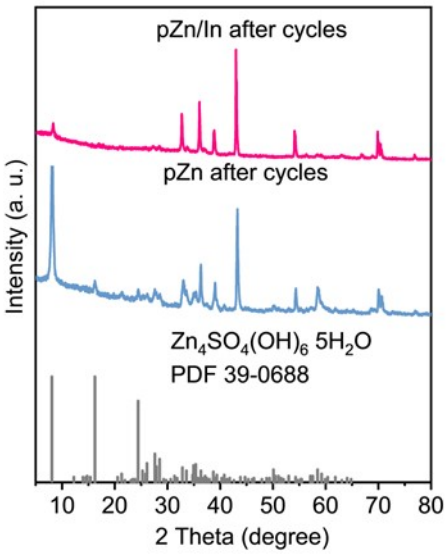

Fig. S19. The corresponding XRD patterns of the bare pZn and pZn/In after cycles.

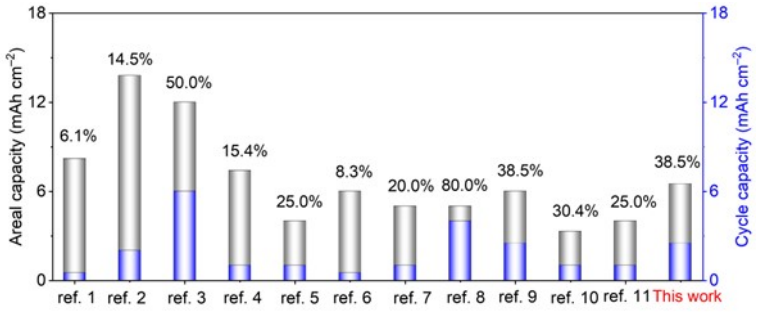

Fig. S20. Zn utilization rate comparison in Zn||Zn symmetric cells between this work and other reported studies.[1–11]

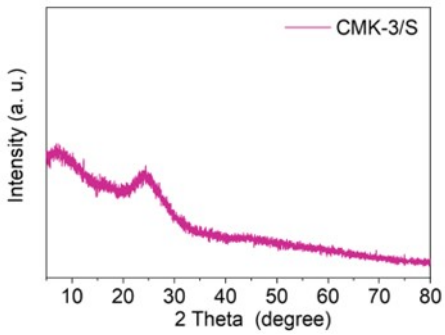

Fig. S21. XRD pattern of CMK-3/S.

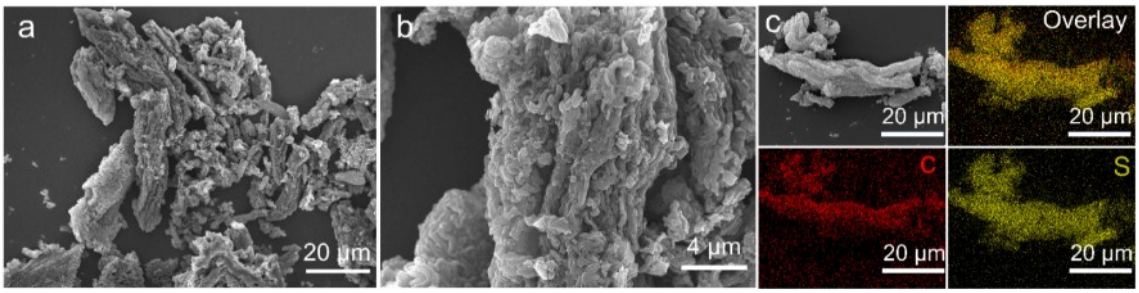

Fig. S22. SEM images and the related elemental mapping images of CMK-3/S.

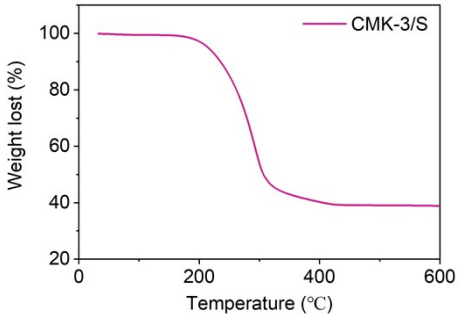

Fig. S23. TGA curves of the CMK-3/S.

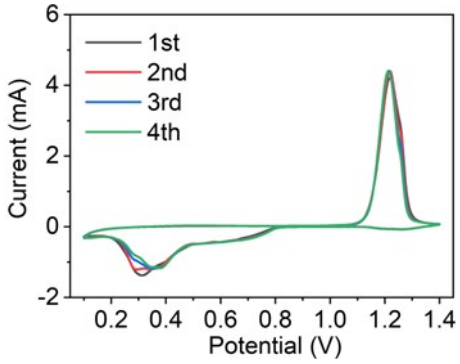

Fig. S24. The CV curves of Zn−S full cells with pZn/In anode at a scan rate of 0.1 mV s^{-1}.

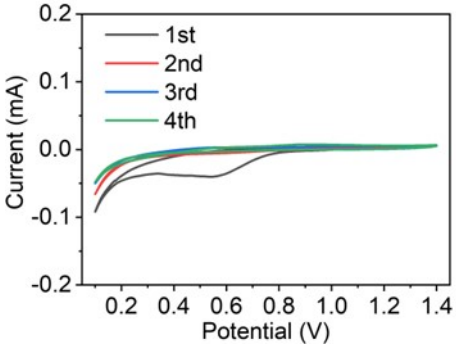

Fig. S25. The CV curves of Zn−S full cells without ZnI_2 additive at a scan rate of 0.1 mV s^{-1}.

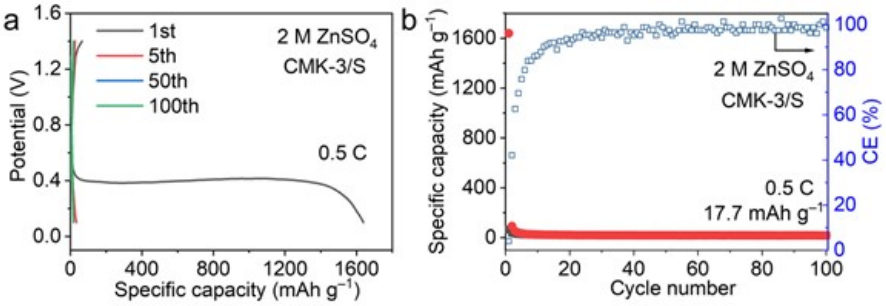

Fig. S26. The voltage profiles and the cycling performance of Zn–S full cell without ZnI_2 additive at 0.5 C.

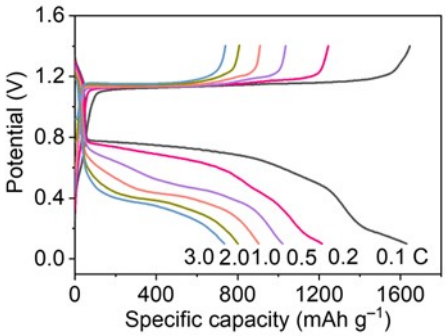

Fig. S27. The voltage profiles of Zn–S full cell with pZn/In anode at current rates from 0.1 C to 3 C.

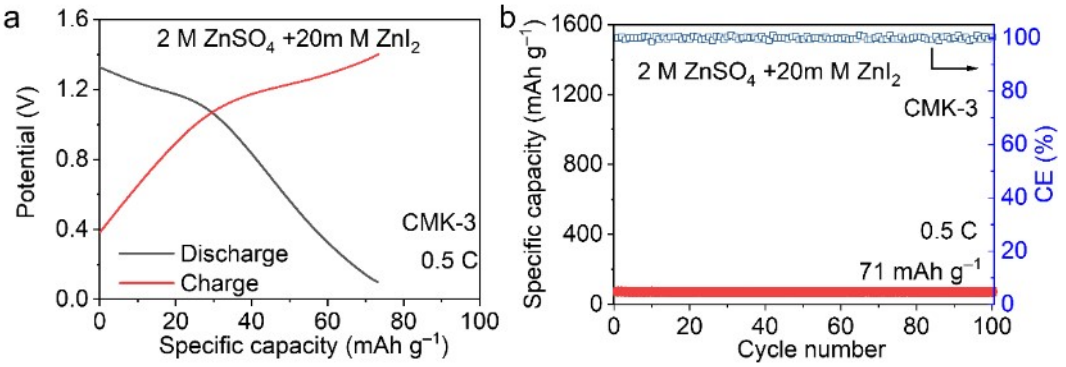

Fig. S28. The charge-discharge curves and the related cycling performance of CMK-3 electrode in the electrolyte of 2 M $ZnSO_4$ + 20 mM ZnI_2 at 0.5 C.

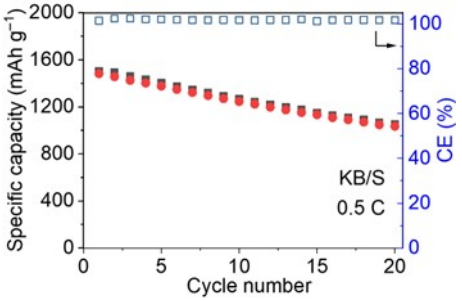

Fig. S29. The cycling performance of Zn–S full cell with KB/S cathode at 0.5 C.

Table S1. Performance comparison of finite Zn anode and Zn DOD in full cells between this work and other reported studies.

Finite Zn anode	Area loading (mAh cm^{-2})	Test condition	Cycling life (h)	Depth of Discharge (DOD)	Cathode (loading)	Zn DOD in full cells
Zn-P-MIEC[1]	13.8	(5.0 mA cm^{-2}, 2.0 mAh cm^{-2})	180	14.5 %	MnO_2 (1 mg cm^{-2})	2.0 %
MXene@Zn[2]	8.2	(1.0 mA cm^{-2}, 0.5 mAh cm^{-2})	200	6.1%	FeHCF, MnO_2	Unavailable

Sn@NHCF-Zn[3]	12.0	(3.0 mA cm^{-2}, 6.0 mAh cm^{-2})	100	50%	V_2O_5（1.2 mg cm^{-2})	2.4 %
Zn powder/PG[4]	7.38	(1.0 mA cm^{-2}, 1.0 mAh cm^{-2})	400	15.4%	MnO_2 (1~3 mg cm^{-2})	5%~15.4 %
$Ti_3C_2T_x$ MXene@Zn[5]	4.0	(1.0 mA cm^{-2}, 1.0 mAh cm^{-2})	300	25%	$LiMn_2O_4$ (1.5~2 mg cm^{-2})	3%~4.0 %
3D Porous Cu Skeleton[6]	6.0	(0.5 mA cm^{-2}, 0.5 mAh cm^{-2})	350	8.3%	MnO_2 (0.9~1.1 mg cm^{-2})	5.83%
Cu foam@Zn[7]	5.0	(2.0 mA cm^{-2}, 1.0 mAh cm^{-2})	150	20.0%	MnO_2	Unavailable
Cu-Zn@Cu mess[8]	5.0	(2.0 mA cm^{-2}, 4.0 mAh cm^{-2})	240	80%	MnO_2	Unavailable
Zn/CNT[9]	6.5	(5.0 mA cm^{-2}, 2.5 mAh cm^{-2})	150	38.5%	CNT-MnO_x@PEDOT (4.3 mg cm^{-2})	19.8%
Zn@N-VG@CC[10]	3.28	(1.0 mA cm^{-2}, 1.0 mAh cm^{-2})	65	30.4%	MnO_2@N-VG@CC (~0.7 mg cm^{-2})	~5.8%
Zn@NSH[11]	4	(10.0 mA cm^{-2}, 1.0 mAh cm^{-2})	110	25%	MnO_2 (2–3 mg cm^{-2})	14~21%
pZn/In This work	6.5	(10.0 mA cm^{-2}, 2.5 mAh cm^{-2})	285	38.5%	S (2 ~2.5 mg cm^{-2})	~54%

Table S2. The performance comparison with the reported Zn-S batteries.

Anode (Thickness or Area loading)	Cathode (loading mg cm^{-2})	Electrolyte	Performance
Zn foil (Unavailable)[12]	S@CNTs-50 (3–5 mg cm^{-2})	1M $Zn(CH_3COO)_2$ + 0.05 wt% I_2	302 mAh g^{-1} after 225 cycles at 2 A g^{-1}
Zn foil (100 μm)[13]	S@C (1.0-1.5 mg cm^{-2})	0.5 M $ZnCl_2$+0.5 M LiCl in deep eutectic solvent (urea: choline=2:1) +10% acetonitrile	126.1 mA h g^{-1} after 400 cycles at 1.0 A g^{-1}
Zn foil (300 μm)[14]	(poly(Li_2S_6-r-DIB)copolymer (4 mg cm^{-2})	1 M $Zn(TFSI)_2$ + 21 M LiTFSI	204 mAh g^{-1} after 1600 cycles at 1 A g^{-1}
Zn foil (100 μm)[15]	ZnS@CF (1.5–3 mg cm^{-2})	3 M $ZnSO_4$ + 1 wt% TU	226 mAh g^{-1} after 300 cycles at 2 A g^{-1}
Zn foil (300 μm)[16]	HCS/S (1.2–1.6 mg cm^{-2})	2 M $Zn(OTF)_2$ + 40% (vol) tetraglyme/water + 0.15 wt % I_2	347 $mAhg^{-1}$ after 600 cycles at 4 A g^{-1}
Zn foil (Unavailable)[17]	S@Fe-PANi (1.8 mg cm^{-2})	2 M $ZnSO_4$	605.7 $mAhg^{-1}$ after 200 cycles at 0.5 A g^{-1}.
Zn foil (Unavailable)[18]	S@CNTs-50 (1.5–2.5 mg cm^{-2})	1 M $Zn(CH_3COO)_2$ + PEG-400 (mass ratio to water = 5:2) + 0.05 wt% I_2	645 mAh g^{-1} after 300 cycles at 1 A g^{-1}.
pZn/In (6.5 mAh cm^{-2}) This work	CMK-3/S (2.0–2.5 mg cm^{-2})	2 M $ZnSO_4$ + 20 mM ZnI_2	271 mAh g^{-1} after 300 cycles at 3.35 A g^{-1} (2C)

References

1. M. Zhang, P. F. Yu, K. R. Xiong, Y. Y. Wang, Y. L. Liu and Y. R. Liang, *Adv. Mater.*, 2022, **34**, 2200860.
2. X. L. Li, Q. Li, Y. Hou, Q. Yang, Z. Chen, Z. D. Huang, G. J. Liang, Y. W. Zhao, L. T. Ma, M. Li, Q. Huang and C. Y. Zhi, *ACS Nano*, 2021, **15**, 14631–14642.
3. H. Yu, Y. X. Zeng, N. W. Li, D. Y. Luan, L. Yu and X. W. (David) Lou, *Sci. Adv.*, 2022, **8**, eabm5766.
4. W. C. Du, S. Huang, Y. F. Zhang, M. H. Ye and C. C. Li, *Energy Stor. Mater.*, 2022, **45**, 465–473.

5. Y. Tian, Y. L. An, C. L. Wei, B. J. Xi, S. L. Xiong, J. K. Feng and Y. T. Qian, *ACS Nano*, 2019, **13**, 11676−11685.
6. Z. Kang, C. L. Wu, L. B. Dong, W. B. Liu, J. Mou, J. W. Zhang, Z. W. Chang, B. Z. Jiang, G. X. Wang, F. Y. Kang and C. J. Xu, *ACS Sustainable Chem. Eng*., 2019, **7**, 3364−3371.
7. C. P. Li, X. D. Shi, S. Q. Liang, X. M. Ma, M. M. Han, X. W. Wu and J. Zhou, *Chem. Eng. J.*, 2020, **379**, 122248.
8. Q. Zhang, J. Y. Luan, L. Fu, S. A. Wu, Y. G. Tang, X. B. Ji and H. Y. Wang, *Angew. Chem. Int. Ed.*, 2019, **58**, 15841–15847.
9. Y. X. Zeng, X. Y. Zhang, R. F. Qin, X. Q. Liu, P. P. Fang, D. Z. Zheng, Y. X. Tong and X. H. Lu, *Adv. Mater.*, 2019, **31**, 1903675.
10. Q. H. Cao, H. Gao, Y. Gao, J. Yang, C. Li, J. Pu, J. J. Du, J. Y. Yang, D. M. Cai, Z. H. Pan, C. Guan and W. Huang, *Adv. Funct. Mater.*, 2021, **31**, 2103922.
11. Q. P. Jian, Z. X. Guo, L. C. Zhang, M. C. Wu and T. S. Zhao, *Chem. Eng. J.*, 2021, **425**, 130643.
12. W. Li, K. L. Wang and K. Jiang, *Adv. Sci.*, 2020, **7**, 2000761.
13. M. W. Cui, J. B. Fei, F. N. Mo, H. Lei, and Y. Huang, *ACS Appl. Mater. Interfaces*, 2021, **13**, 54981−54989.
14. Y. W. Zhao, D. H. Wang, X. L. Li, Q. Yang, Y. Guo, F. N. Mo, Q. Li, C. X. Peng, H. F. Li and C. Y. Zhi, *Adv. Mater.*, 2020, **32**, 2003070.
15. D. D. Liu, B. He, Y. Zhong, J. Chen, L. X. Yuan, Z. Li and Y. H. Huang, *Nano Energy*, 2022, **101**, 107474.
16. M. Yang, Z. C. Yan, J. Xiao, W. L. Xin, L. Zhang, H. L. Peng, Y. H. Geng, J. W. Li, Y. X. Wang, L. Liu and Z. Q. Zhu, *Angew Chem. Int. Ed.*, 2022, **61**, e202212666.
17. H. Zhang, Z. T. Shang, G. Luo, S. H. Jiao, R. G. Cao, Q. W. Chen and K. Lu, *ACS Nano*, 2022, **16**,

7344–7351.

18. T. S. Zhou, H. Wan, M. K. Liu, Q. Y. Wu, Z. C. Fan and Y. C. Zhu, *Mater. Today Energy*, 2022, **27**, 101025.